AJNR

Contrast-enhanced MR Angiography: The Effects of k-Space Truncation on Luminal Representation in a Carotid Artery Phantom Model

Elias R. Melhem, Jean-Micheal Serfaty, Lisa Jones, Ryuta Itoh, Brian S. Kuszyk, Jean-Baptiste Martin, Philippe Gailloud, Kieran P.J. Murphy and Daniel A. Rufenacht

AJNR Am J Neuroradiol 2000, 21 (6) 1028-1031
http://www.ajnr.org/content/21/6/1028

AJNR Am J Neuroradiol 21:1028–1031, June/July 2000

Technical Note

Contrast-enhanced MR Angiography: The Effects of k-Space Truncation on Luminal Representation in a Carotid Artery Phantom Model

Elias R. Melhem, Jean-Micheal Serfaty, Lisa Jones, Ryuta Itoh, Brian S. Kuszyk, Jean-Baptiste Martin, Philippe Gailloud, Kieran P.J. Murphy, and Daniel A. Rufenacht

Summary: Using carotid bifurcation phantom models with different degrees of stenoses, we evaluated the accuracy of vessel lumen representation on MR images obtained from the inverse Fourier transform of different k-space percentages. Our results show that the lower thresholds of truncated k-space sampling are dictated by the severity of luminal narrowing. The defined thresholds may help improve efficiency of 3D MR imaging of the carotid arteries while maintaining adequate luminal representation.

The need for noninvasive imaging of the carotid arteries has provided fertile ground for the rapid development and application of different MR angiographic techniques (1, 2). Contrast-enhanced MR angiographic techniques (using T1-shortening agents) have shown potential for accurate representation of the vascular lumen compared with conventional angiography (3).

Carotid imaging using contrast-enhanced 3D MR angiography has followed one of three trends: 1) ultra-high spatial resolution imaging with low temporal resolution, necessitating, at times, tedious image postprocessing for the extraction of the carotid arteries from superimposed capillaries and veins (3); 2) high spatial and temporal resolution imaging, requiring different schemes for timing the arrival of the contrast bolus to coincide with the center of k-space (4); 3) ultra-high temporal resolution (<6 s) imaging (bolus tracking) with submillimeter in-plane resolution that requires little image postprocessing and no contrast bolus timing. In the latter method, improvements in temporal resolution are often the result of partial k-space updating for each dynamic acquisition (keyhole) (5, 6).

In addition to anatomic display of the carotid arteries, ultra-fast contrast-enhanced 3D MR angiography can provide information regarding flow dynamics in the cervical vasculature. Also, it can reduce motion-related artifacts and obviate the need for cumbersome image postprocessing and for high doses of contrast agent (7).

Using carotid bifurcation phantom models with different degrees of stenosis at the origin of the internal carotid arteries, we evaluated the accuracy of vessel lumen representation on images obtained from the inverse Fourier transform of different k-space percentages. Using fixed concentrations of contrast material and a steady-state flow model, we aimed to define a minimum k-space percentage below which vessel lumen representation becomes distorted.

Methods

MR Imaging

MR studies were performed on a 1.5-T superconducting MR system (ACS NT Power Trak 6000; Philips Medical Systems, Shelton, CT) with maximum gradient capability of 23 $mT.m^{-1}$ and a slew rate of 103 $mT.m^{-1}.ms^{-1}$. MR images were obtained with a standard quadrature head coil operating in receive mode.

The MR angiographic technique implemented a 3D fast field-echo readout, with 4.4/1.5 (TR/TE) (partial echo sampling), a flip angle of 30°, and a readout bandwidth of 450 Hz per pixel. Complete coverage of the carotid phantoms was achieved in the coronal plane by using a single 4.1-cm-thick volume with an in-plane field of view of 25 cm and a matrix of 256 × 256. The volume thickness was divided into 55 1.5-mm-thick partitions reduced to an effective thickness of 0.75 mm by using interpolation (zero filling) in the section direction. Acquisition time was 62 s.

Phantom Models

In vitro models of common carotid bifurcations were derived from a vascular cast of the cervicocranial arteries obtained on an unfixed human specimen. A mixture of methylmethacrylate and barium sulfate powder was injected in the proximal descending thoracic aorta under continuous fluoroscopic control. The specimen was then maintained in a 15% solution of potassium hydroxide until complete dissolution of the surrounding soft and bony tissues occurred. Multiple wax copies of the arterial cast were produced by applying a molding procedure adapted from dentistry prosthetic techniques.

Four stenotic lesions of increasing severity were simulated by remodeling the carotid bifurcation of otherwise identical wax copies. These wax copies were then coated with liquid silicone and placed in a 3D rotator device, ensuring even dis-

Received September 3, 1999; accepted after revision January 7, 2000.

From the Department of Radiology and Radiological Sciences (E.R.M., J.-M.S., L.J., R.I., B.S.K., P.G., K.P.J.M.), The Johns Hopkins Hospital, Baltimore, MD, and the Department of Radiology (J.-B.M., D.A.R.), Geneva University Hospital, Geneva, Switzerland.

Address reprint requests to the Department of Radiology, The Johns Hopkins Hospital, 600 North Wolfe Street, Baltimore, MD 21287.

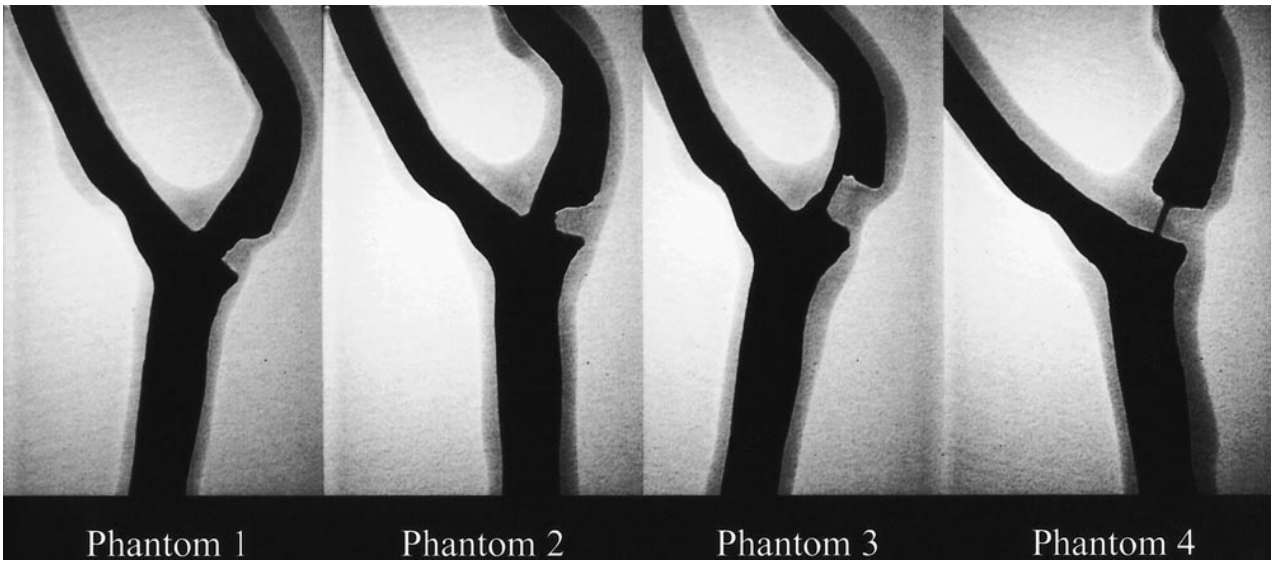

FIG 1. Digital radiographs of the iodinated contrast-material–filled carotid artery phantom models. The measured degree of stenosis is 38% for phantom 1, 61% for phantom 2, 80% for phantom 3, and 92% for phantom 4.

tribution of the silicone during the drying process. The models were exposed to high temperature (80°C) to evacuate the wax by melting.

The finished models were filled with iodinated contrast material and imaged using digital radiography (field of view, 15 cm; matrix, 1024 × 1024) at different obliquities to optimize visualization of the stenotic segment (Fig 1). With the optimal obliquity, the stenotic lesions were measured using caliper tools found on a commercially available on-line workstation. For each of the four phantoms, the percent stenosis was measured by comparing the diameter of the stenotic segment to the normal distal segment (NASCET method). The degree of stenosis was 38% for phantom 1, 61% for phantom 2, 80% for phantom 3, and 92% for phantom 4. Values derived by the evaluation of luminal representation on MR angiograms were considered to be the standard of reference. For the MR imaging experiments, a contrast material and water solution (126.42/105.71 [T1/T2]) was infused through the phantom models at a fixed flow rate of 85 mL/s by using a calibrated motorized pump.

Data Analysis and Postprocessing

The 3D MR angiographic data obtained from the four phantoms were transferred to an off-line workstation. Using a program written in interactive data language, low passed versions of the entire data corresponding to 0, 10, 20, etc., to 100% k-space were calculated. These low-passed versions were generated by retaining a central cube of the appropriate percent of k-space while zeroing outside this central region. MR angiographic images were generated from the inverse Fourier transform of the different k-space percentages and were displayed using a standard maximum intensity projection ray-trace algorithm (Figs 2 and 3). The maximum intensity projections of the four phantoms were rotated to match the obliquity of the standard of reference visually.

The degree of luminal stenosis in the four phantoms was calculated according to the NASCET method for the different k-space percentages. The luminal diameter was measured using the number of pixels with signal intensity above half maximum in the line profile drawn perpendicular to the vessel. In situations in which the stenotic segment was not identifiable because of either complete signal drop off or obscuration, the luminal diameter was arbitrarily set to zero.

The ratio of luminal stenoses (MR angiography/standard of reference) was plotted as a function of percent k-space. This was done to determine a percent k-space threshold below which MR angiographic revelation of luminal stenosis becomes distorted. Distortion of luminal stenosis on MR angiograms was arbitrarily defined as a ratio more than 15% different from unity (<0.85 or >1.15) based on the shape of the plot.

Results

MR angiographic images of the four phantoms obtained from the inverse Fourier transform of the entire k-space data showed luminal stenosis within 15% of the standard of reference (Fig 4). For phantom 1, adequate luminal stenosis representation (ratio, 1.14) was maintained despite using only the central 30% of k-space data. Below this threshold, image distortion led to inadequate luminal representation (Fig 4). The thresholds for phantoms 2, 3, and 4 were 40%, 40%, and 60% k-space, respectively. At these thresholds, the ratio of luminal stenosis for phantom 2 was 1.03, for phantom 3 was 0.90, and for phantom 4 was 0.93. Below these thresholds, image distortion resulted in poor luminal representation (Fig 4). There were no appreciable differences in luminal stenosis representation of the four phantoms as we decreased the percent k-space from 100% to the respective thresholds (Fig 4).

Discussion

High spatial frequency data found in the periphery of k-space is responsible for image detail, whereas low spatial frequency data found in the center of k-space is responsible for image contrast. Limiting the signal sampling process to the central portions of k-space improves the efficiency of scanning at the expense of image detail and spatial resolution (4, 6, 8).

For accurate luminal representation, our phantom experiments show that as the severity of stenosis

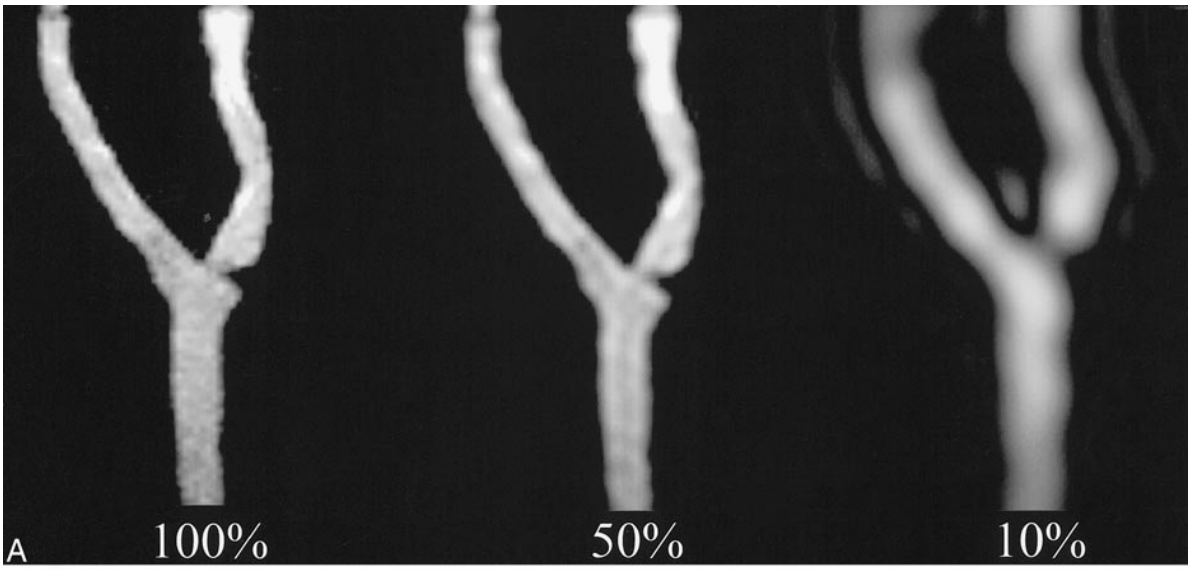

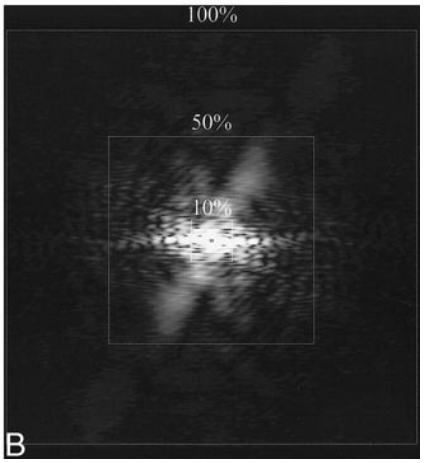

FIG 2. 2D projectional images of 3D k-space data. *A,* Superimposed *squares* show the percentages of k-space used to generate corresponding different MR angiographic maximum intensity projections (4.1/1.5, flip angle of 30°) of the phantom. *B,* Inverse Fourier transform of 2D projectional image is an MR angiographic image of phantom 2. Adequate luminal representation is maintained at 50% k-space, but is lost at 10% k-space.

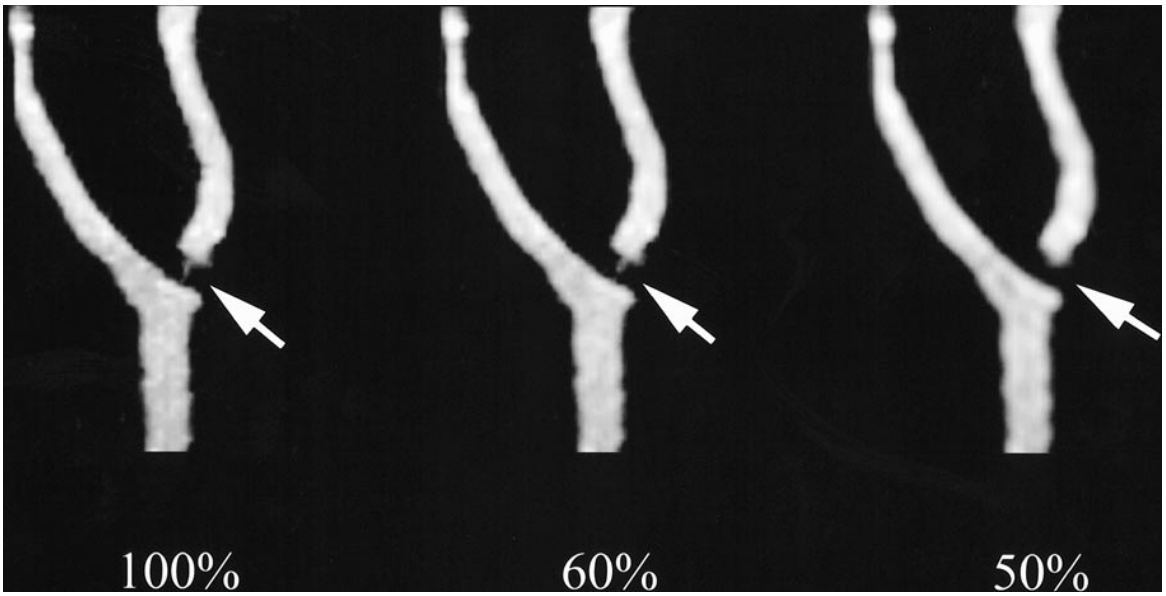

FIG 3. MR angiographic maximum intensity projections (4.1/1.5, flip angle of 30°) of phantom 4 show that luminal representation is maintained at 60% k-space, but is lost at 50% k-space (*arrows*).

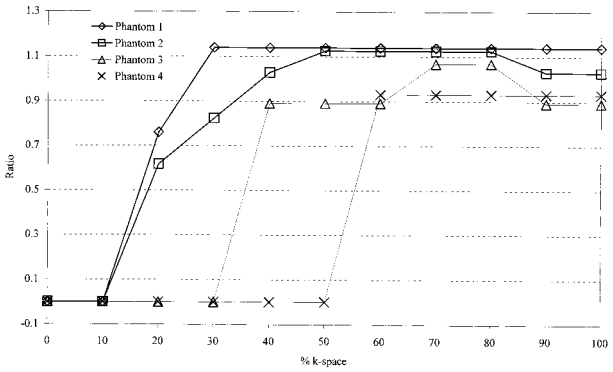

FIG 4. Plot of the ratio of luminal stenosis in the four phantoms shown by MR angiography (4.1/1.5, flip angle of 30°) divided by the standard of reference as a function of percent k-space. The ratio deviates from unity at higher percent k-space for phantoms with greater severity of stenosis.

increases, so does the need for a larger percentage of k-space sampling. In the case of phantom 4 (92% stenosis), at least 60% of the central portion of k-space is required for accurate representation, whereas for phantom 1 (38% stenosis), only 30% is needed. This can be explained in that high spatial frequency data (periphery of k-space), responsible for image detail, become more critical for the revelation of small structures, such as severely stenotic segments.

Despite the severe narrowing in phantom 4, we were able to reduce k-space sampling by 40% and still maintain accurate luminal representation. This reduction in k-space sampling at the above-specified MR imaging spatial resolution and for the most extreme situation tested, allows a commensurate decrease in acquisition time (5).

Ultra-fast contrast-enhanced 3D MR angiography (<6 s/dynamic) has several advantages in carotid imaging. It allows the study of flow dynamics in the cervical and intracranial circulation, provides a reliable method to time-resolve the carotid arteries from the jugular vein, reduces motion-related artifacts, and allows decreases in the total dose of contrast agent required for the same intraluminal signal-to-noise ratio (7). The latter advantage is based on the approximation that for a particular injection rate, the duration of the peak intraarterial concentration of contrast agent is proportional to the total dose administered (3).

The combination of high-performance gradients (hardware) and different k-space truncation schemes (software) have shown potential for high temporal resolution MR angiography with sufficient spatial resolution for carotid imaging (6). We think that our results can help guide efforts aimed at improving imaging efficiency without significantly sacrificing anatomic information.

Our results are limited in part by the inability of the phantom model to emulate carotid arteries in vivo accurately. Nevertheless, the phantom models that are used in this experiment have been shown to be anatomically accurate and reproducible with viscoelastic properties very similar to those of real human carotid arteries (9). Further, the viscosity of the contrast material solution used in the experiments is different from that of blood and the motorized flow pump does not provide pulsatile flow. The effects of viscosity and pulsatile flow on intravoxel phase dispersion and vascular lumen response cannot be addressed in this study. Finally, the use of maximum intensity projection MR images for measuring the degree of stenosis and the use of different methods to measure the degree of stenosis on the fluoroscopic images and MR images may have influenced our results.

Conclusion

Truncated k-space sampling in MR angiography leads to improvements in time resolution without necessarily compromising anatomic information. Lower thresholds of k-space sampling are dictated by the severity of narrowing. Our results can help guide efforts aimed at improving the efficiency of 3D MR imaging of the carotid arteries.

References

1. Mayberg MR, Winn HR. **Endarterectomy for asymptomatic carotid artery stenosis: resolving the controversy.** *JAMA* 1995; 273:1459–1461
2. Goodson SF, Flanigan DP, Bishara RA, Schuler JJ, Kikta MJ, Meyer JP. **Can carotid duplex scanning supplant arteriography in patients with focal carotid territory symptoms?** *J Vasc Surg* 1987;5:551–557
3. Prince MR, Yucel EK, Kaufman JA, Harrison DC, Geller SC. **Dynamic gadolinium-enhanced three-dimensional abdominal MR arteriography.** *J Magn Reson Imaging* 1993;3:877–881
4. Huston J III, Fain SB, Riederer SJ, Wilman AH, Bernstein MA, Busse RF. **Carotid arteries: maximizing arterial to venous contrast in fluoroscopically triggered contrast-enhanced MR angiography with elliptic centric view ordering.** *Radiology* 1999; 211:265–273
5. Korosec FR, Frayne R, Grist TM, Mistretta CA. **Time-resolved contrast-enhanced 3D MR angiography.** *Magn Reson Med* 1996;36:345–351
6. Melhem ER, Caruthers SD, Faddoul SG, Tello R, Jara H. **Use of three-dimensional MR angiography for tracking a contrast bolus in the carotid artery.** *AJNR Am J Neuroradiol* 1999;20:263–266
7. Lee VS, Rofsky NM, Krinsky GA, et al. **Single dose gadolinium-enhanced 3D-MR angiography of the renal arteries optimized with a timing examination: effects of injection rate, patient circulation time, and breath-holding.** *Radiology* 1998;209P: 177[Suppl S]
8. Fain SB, Riederer SJ, Bernstein MA, Huston J III. **Theoretical limits of spatial resolution in elliptical-centric contrast-enhanced 3D-MRA.** *Magn Reson Med* 1999;42:1106–1116
9. Gailloud P, Muster M, Piotin M, et al. **In vitro models of intracranial arteriovenous fistulas for the evaluation of new endovascular treatment materials.** *AJNR Am J Neuroradiol* 1999;20: 291–295